NRIAG Journal of Astronomy and Geophysics (2013) **2**, 27–38

National Research Institute of Astronomy and Geophysics

NRIAG Journal of Astronomy and Geophysics

www.elsevier.com/locate/nrjag

Analysis of magnetic gradients at North East of Wadi Ar Rika quadrangle, Saudi Arabia, to delineate subsurface linear features and faults

Maha Abdelazeem [a,*], **El-Sawy K. El-Sawy** [b,1], **Mohamed M. Gobashy** [b,2]

[a] *National Research Institute of Astronomy and Geophysics (NRIAG), Egypt*
[b] *Faculty of Earth Sciences, King Abdulaziz University, Jeddah, Saudi Arabia*

Received 23 October 2012; accepted 30 January 2013
Available online 2 July 2013

Abstract Ar Rika fault zone constitutes one of the two major parts of the NW–SE Najd fault system (NFS), which is one of the most prominent structural features located in the east of the center of the Arabian Shield, Saudi Arabia. By using Enhancement Thematic Mapper data (ETM^+) and Principle Component Analysis (PCA), surface geological characteristics, distribution of rock types, and the different trends of linear features and faults are determined in the study area. First and second order magnetic gradients of the geomagnetic field at the North East of Wadi Ar Rika have been calculated in the frequency domain to map both surface and subsurface lineaments and faults. Lineaments as deduced from previous studies, suggest an extension of the NFS beneath the cover rocks in the study area. In the present study, integration of magnetic gradients and remote sensing analysis that resulted in different valuable derivative maps confirm the subsurface extension of some of the surface features. The 3D Euler deconvolution, the total gradient, and the tilt angle maps have been utilized to determine accurately the distribution of shear zones, the tectonic implications, and the internal structures of the terranes in the Ar Rika quadrangle in three dimensions.

* Corresponding author.
E-mail address: maazeem03@hotmail.com (M. Abdelazeem).
[1] On leave from Faculty of Science, Al-Azhar University, Assiut Branch, Assiut, Egypt.
[2] On leave from Cairo University, Faculty of Science, Cairo, Egypt.
Peer review under responsibility of National Research Institute of Astronomy and Geophysics.

1. Geologic setting

Ar Rika faults are part of the Najd fault system (NFS), which is one of the major structural features in the Arabian Shield (Fig. 1a). It is a system of primary and secondary strike–slip faults, crossing the Arabian Shield and is considered one of the largest recognized Proterozoic transcurrent fault systems with an exposed length of 1100 km and a width of 350 km, extending in a NW direction across the Arabian Shield into Egypt (Moore et al., 1979).

2090-9977 © 2013 Production and hosting by Elsevier B.V. on behalf of National Research Institute of Astronomy and Geophysics.
http://dx.doi.org/10.1016/j.nrjag.2013.06.006

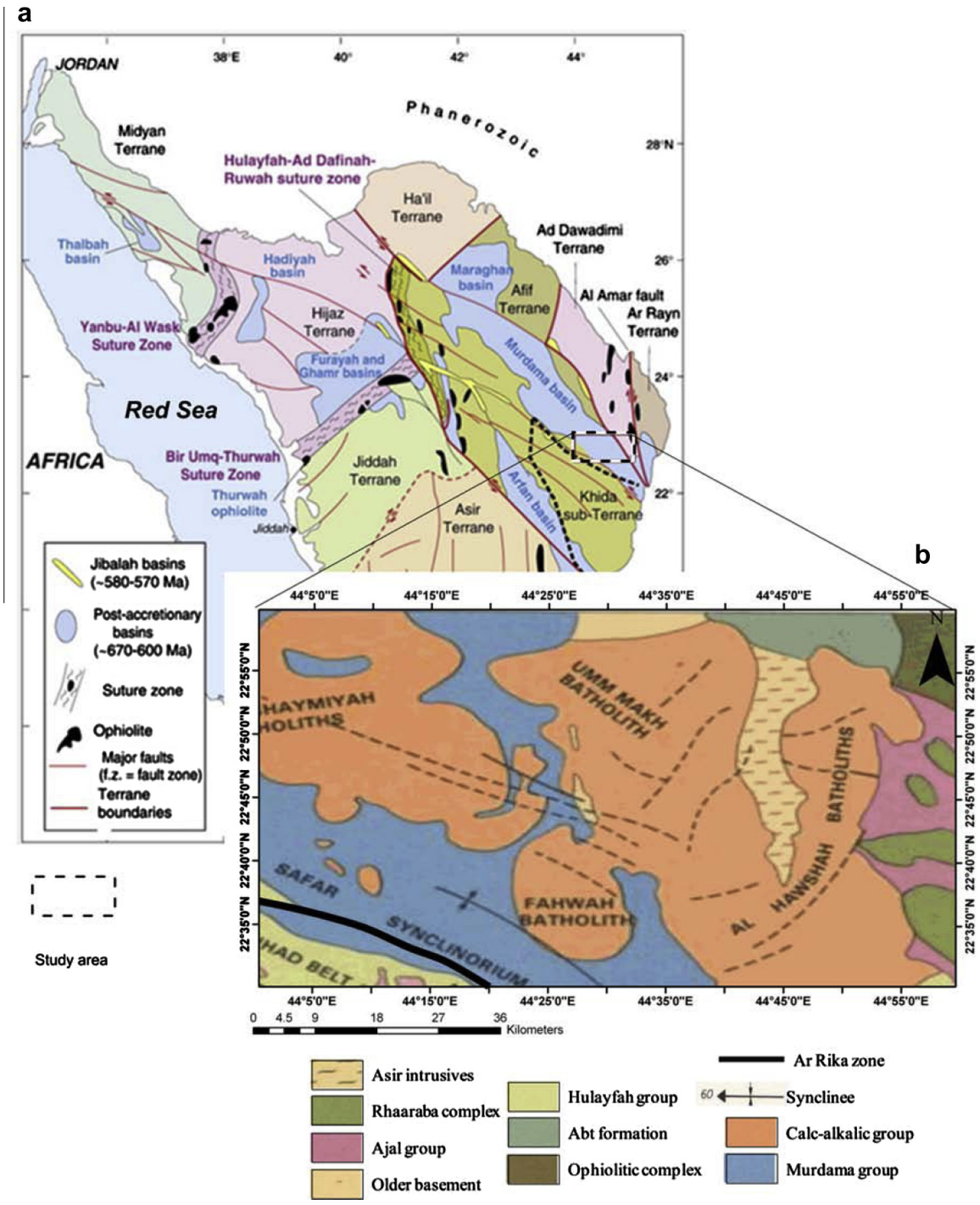

Fig. 1 (a) Simplified map of the Arabian Shield, showing major tectonostratigraphic terranes, ophiolite belts, sutures and fault zones, and post-accretionary basins, modified after Nehlig et al. (2002) and Johnson and Woldehaimanot (2003). (b) Surface geology of the study area (modified after Delfour, 1980).

Along these faults several variations in deformational style are observed: Strike-slip faulting in the northern half of the Shield developed in an environment of higher heat flow and hence was ductile, while the deformation in the crust in the southern half was more brittle (Stern, 1985 and Abdelsalam and Stern, 1996). Individual faults of the Najd system have a maximum left lateral displacement of 65 km in the middle of the Shield (Cole and Hedge, 1986), decreasing toward its edges. Johnson (1996) distinguished between the NW–SE Najd faults based on their origin time, tectonic implications, and associated structures, and gave them two names: Ar Rika and Ruwah faults.

Previous geophysical studies (Mogren et al., 2008) suggest an extension of the Najd system beneath the cover rocks. These shear zones extend southeast for at least 200 km beneath the cover rocks and northwest into Egypt. Generally, Wadi Ar

Table 1 Statistical analysis of lineaments.

Variable	Angles	Variable	Angles
Number of observations	133	Standard error of mean	3.165°
Mean vector (μ)	359.041°	95% Confidence interval (−/+) for μ	352.836°/5.246°
Length of mean vector (r)	0.813	99% Confidence interval (−/+) for μ	350.887°/7.195°
Median	355.486°	Rayleigh test (Z)	87.924
Concentration	3.03	Rayleigh test (p)	0
Circular variance	0.187	ng Test (U)	224.655
Circular standard deviation	36.86°	Rao's Spacing test (p)	<0.01

Rika area is underlain by Precambrian rocks locally covered by thin silt and gravel or by thicker Eolian sand at the base of the foothills. The principal component analysis (Fig. 2) is the result of the application of linear algebra on the ETM$^+$ band, whereas it is considered an optimum approach for separation. The latter depends on the redundant and spectral characteristics of the image (Richards and Jia, 1999). The rock units show a fairly regular distribution along a general northwest trending structure inherited from the main Late Proterozoic phase of folding and fracturing. The relative chronology between the various Precambrian rock units can be distinguished in the field and it has been possible to relate them to the major lithostratigraphic sequences of the northern Arabian Shield (Fig. 3). The oldest unit is the old basement, represented by essentially granitic rocks occupying the northern part of the study area. The former area corresponds to the eastern part of the area of study characterized by several small belts of amphibolites and gneiss (Ajal group) shown in greenish blue (east of the map Fig. 2), and by a fairly continuous 25 km wide northwest trending belt in which numerous layered bodies of gabbro and peridotite (Rharaba complex) are variously digested by granodiorite intrusions of the late Middle Proterozoic age.

Between these two older basement domains units of the Upper Proterozoic age lie in northwest trending belts. They comprise the volcanic sedimentary rocks of the Hulayfah group and the sedimentary sequences of the Murdama group. The Hulayfah group is only represented by the Nuqrah formation that is an assemblage of andesite and rhyolite flows, with related tuff and breccias and minor beds of carbonite rock. The Murdama group rocks (blue color in Fig. 2) in the study area compromise sandstone, greywacke and siltstone, which local polygenic conglomerate and rhyolite or andesite flows. The deformations occurred during the main Ar Rimah phase of folding (prior to 600 m.y.) following which the folded Murdama rocks were cut by large batholiths of the late tectonic to post tectonic granite, ranging in composition from calc-alkalic to alkalic (Kanaan, 1979). Precambrian tectonic activity in the Wadi Ar Rika area ended with epeirogenic movements responsible for the very long fracture seams of the Najd fault system which crosses the Arabian Shield along a northwest strike.

2. Aeromagnetic data

The total filed intensity map of the study area (Longitudes 44° and 45° E, and Latitudes 22° 30′ and 23° N) was digitized to 54×100 data points from the original aeromagnetic map of Saudi Arabia (sheet 129), Ministry of Petroleum and Mineral Resources (1965–1966). The reduced to pole (RTP) map (Fig. 4a) shows a general linear trend NNW–SSE corresponding to the dominant major Najd fault. Surface lineaments for all faults and linear contacts have been extracted from the shaded relied map (0–360°) of the RTP anomalies in Fig. 4a, which are shown in Fig. 4b. The rose diagram and the statistical analysis of the extracted lineaments are shown as subpanel

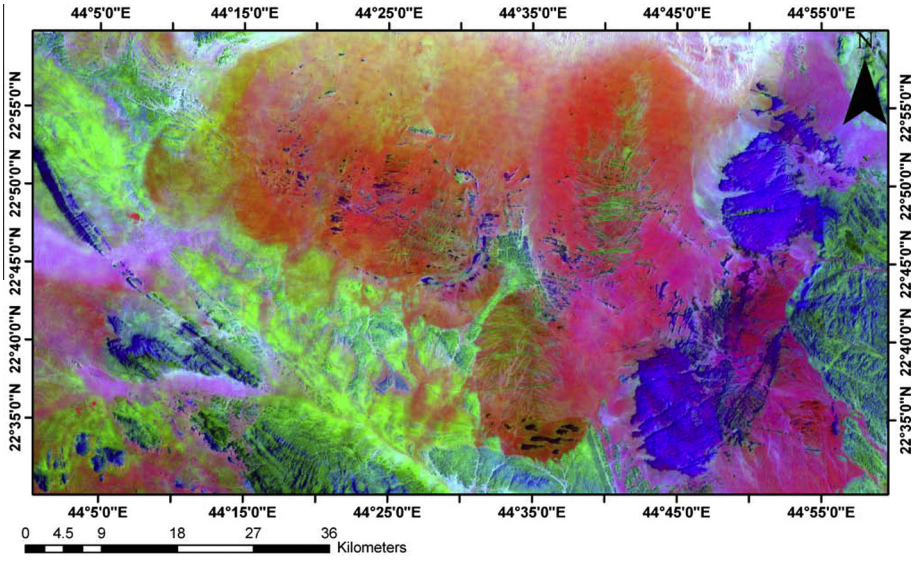

Fig. 2 Image processing principle component analysis (PCA) showing the lithological discrimination of the study area, Saudi Arabia.

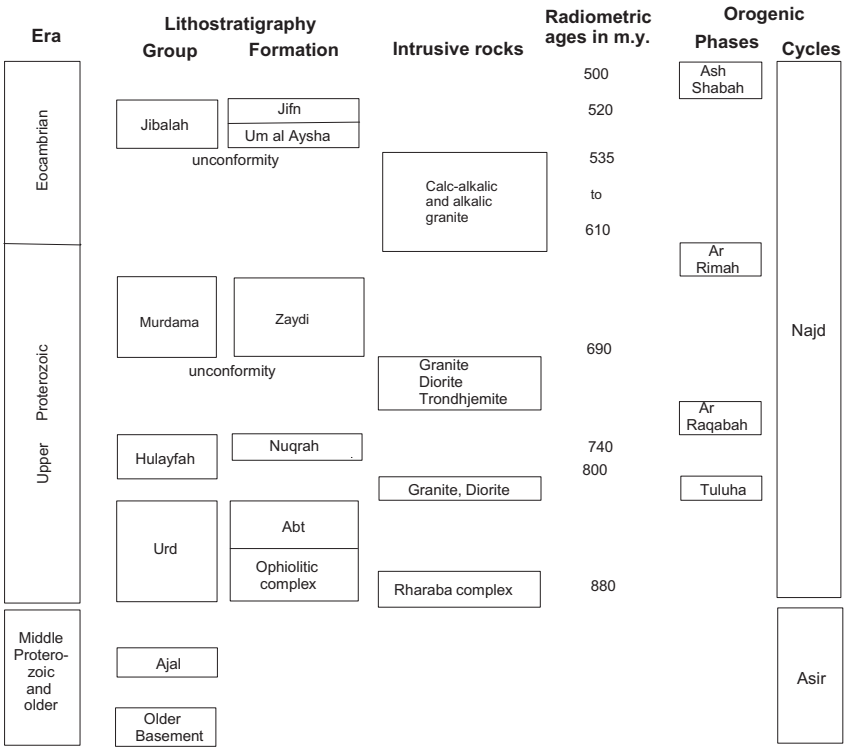

Fig. 3 Lithostratigraphic divisions together with plutonic and tectonic events in the study area and northern Arabian Shield (modified after Delfour, 1980).

in Fig. 4a and Table 1. The most common trends of the area are NW–SE and NE–SW. Structurally, the NE–SW trend is complementary (Delfour, 1980) but less-developed set of faults trends northeast; this can be seen in the Jibal al Hawshah granitic batholiths. The NW-SE trending faults appear to be related to the epeirogenic movements of the Ash Shabah orogenic phase. During this event, very long left-lateral wrench faults, distributed along four major northwest-aligned segments in the northern part of the Arabian Shield, cut the Precambrian basement; these constitute the Najd fault system (NFS). The segment which trends diagonally across the Wadi Ar Rika quadrangle belongs to the southernmost section of this fault system, and is composed of several seams of discontinuous fractures. These are clearly represented in the rose diagram of the RTP map.

Detailed correlation between the surface features and the RTP, shaded relief maps, the surface geology, and the principle component (PCA) map show that: Anomaly (**A**) to the north east of the study area overlaps with the Calc-alkalic granite of Umm Makh and Al Hawshah batholithes. Their magnetic intensity is intermediate (5900–5950 nT in amplitude). Anomaly (**B**) is mainly related to El Fahwah granitic batholiths. It attains maximum amplitude of 6430 nT. Anomaly (**C**), in general is characterized by high frequency texture and comprises many surface structural features. These are, Umm As Safar synclinorium (Murdama group); Al Khushaymyah granitic batholiths; and Al Hawriyah anticlinorium. Anomaly (**D**) corresponds to Gabal Burqah of the Rharaba complex, this is mainly layered gabbro and serpentinized peridotite.

In general, the magnetic anomalies and the surface lineation of the study area are greatly affected by the subsurface segments of three structural provinces that underlie Wadi Ar Rika, lying parallel to each other and trending northwest. These are the Ad Dawadimi Province to the east, the Ad Dafinah Province to the south west, and between them is the ''Afif Province'' which is almost entirely composed of folded Murdama group clastic sediments subsequently intruded by granitic batholiths. These batholiths have a clear signature on the RTP and shaded relief maps.

3. Magnetic data analysis

The main purpose of magnetic data processing is the simplification of the acquired parameters from the observed data. One of these simplification approaches is the creation of a function which is independent to body magnetization direction and ambient geomagnetic parameters. These parameters are important when remnant magnetization is not negligible. Total gradient, and tilt gradients are quantities that include this property and have been used for edge detection and depth estimation of magnetic bodies by several authors. The Ar Rika magnetic map is subjected to filtering techniques in the frequency domain to calculate the different directional derivatives to enhance the structural features in the area and to estimate the depths to causative sources. The 3D Euler is utilized to calculate the depths and to identify the structures and causative source shapes through the automatic identification of the structural index (**SI**). In performing the above gradients several magnetic tensor elements are calculated. The relative importance of each element is evident. The vertical gradients are particularly useful in enhancing the lateral dimensions of anomalous sources (dT/dz). The horizontal gradient, $\boldsymbol{h}(x,y) = [(d^2T/dx^2)^2 + (d^2T/dy^2)^2]^{1/2}$, total gradient $\boldsymbol{a}(x,y) =$

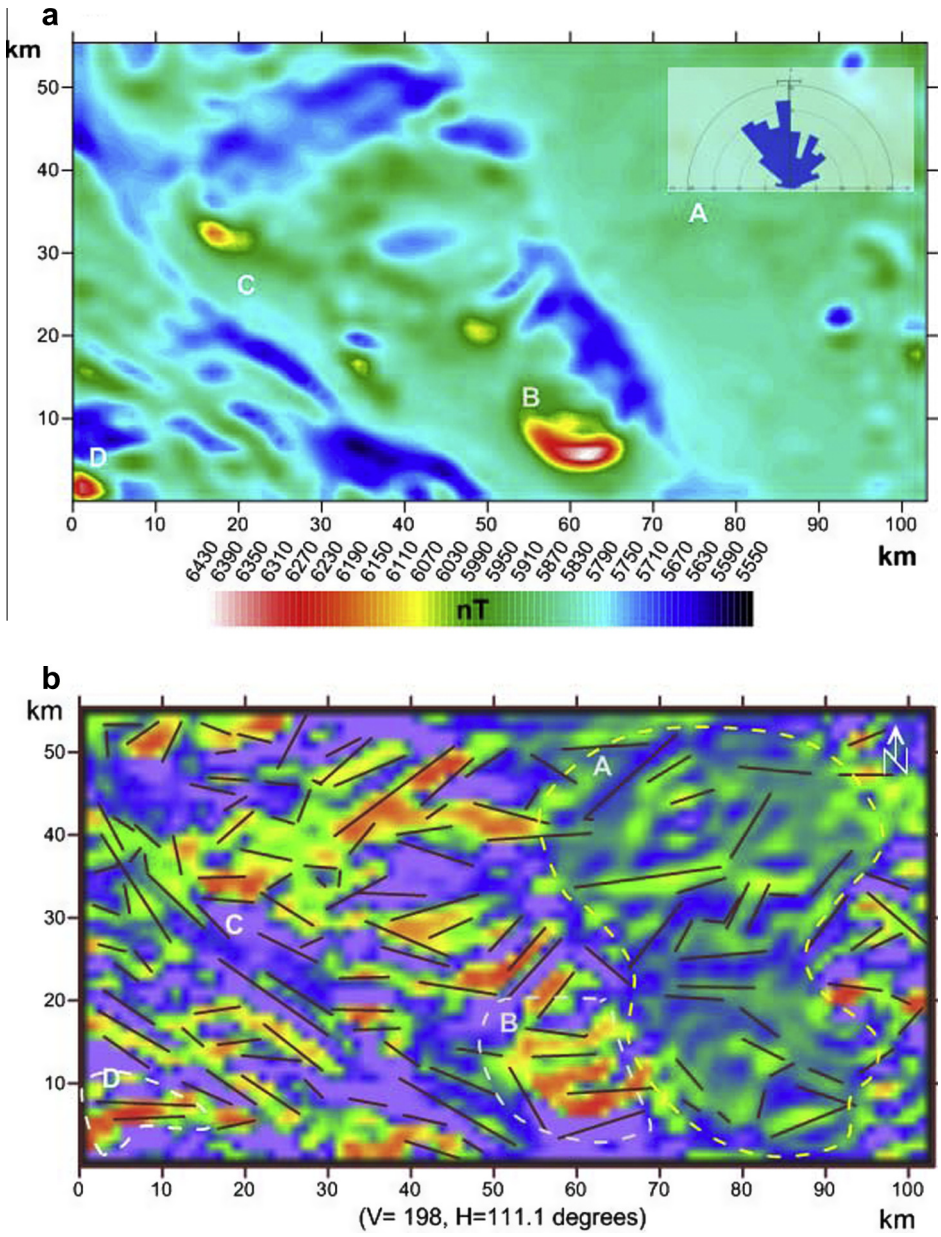

Fig. 4 (a) Reduced to pole (RTP) with a frequency analysis shown in the rose diagram at the top right corner. (b) Shaded relief map for the study area. Extracted surface lineaments are posted on.

$[d^2T/dx^2 + d^2T/dy^2 + d^2T/dz^2]^{1/2}$ (also known as analytical signal), and the tilt gradient $\boldsymbol{t}(x,y) = \arctan [dT/dz/h(x,y)]$ are useful operations that can be used in the visual interpretation of magnetic maps. Fig. 5(a, b, c, d and f) shows the calculated components $\boldsymbol{T}_{xx}$, $\boldsymbol{T}_{yy}$, $\boldsymbol{T}_{zz}$, $\boldsymbol{h}$, and $\boldsymbol{a}$. Moreover, we calculate the magnetic potential as long as it is primarily used in the process of *FFT* transformation. The magnetic potential (Fig. 5a) shows high anomaly over the Murdama group and the Umm Makh and Al Hawshah batholithes. Also an evident large potential can be observed overlying El Fahwah granitic batholiths to the south of the study area. All gradient anomalies reflect evidences of lateral magnetic susceptibility contrasts in the surface/or subsurface rock units in the study area. These generally trend NW–SE (Fig. 6). For the $\boldsymbol{T}_{xx}$ anomaly, the mean vector is 105.6 degrees; for the $\boldsymbol{T}_{yy}$ anomaly, the mean vector is 165.2 degrees, and for the $\boldsymbol{T}_{zz}$ anomaly the average mean direction is 152 degrees. Such qualitative analysis suggests remarkable subsurface extension of the surface lineaments and faults. The automated interpretation of potential field data is usually aided by evaluating the curvature of special functions of the data that peak over sources such as contacts and faults (Phillips et al., 2007). The horizontal gradient ($\boldsymbol{h}$) and the total gradient ($\boldsymbol{a}$) are among these special functions. Both are calculated as mentioned in the previous sections. The results are show in Fig. 5e and f. Directional analysis of the extracted linear features (Fig. 6) correlates well with the $\boldsymbol{T}_{xx}$, $\boldsymbol{T}_{yy}$, $\boldsymbol{T}_{zz}$ anomalies (mean vector 136.04 degrees for total gradient ($\boldsymbol{a}$) and 118.9 degrees for horizontal gradient ($\boldsymbol{h}$).

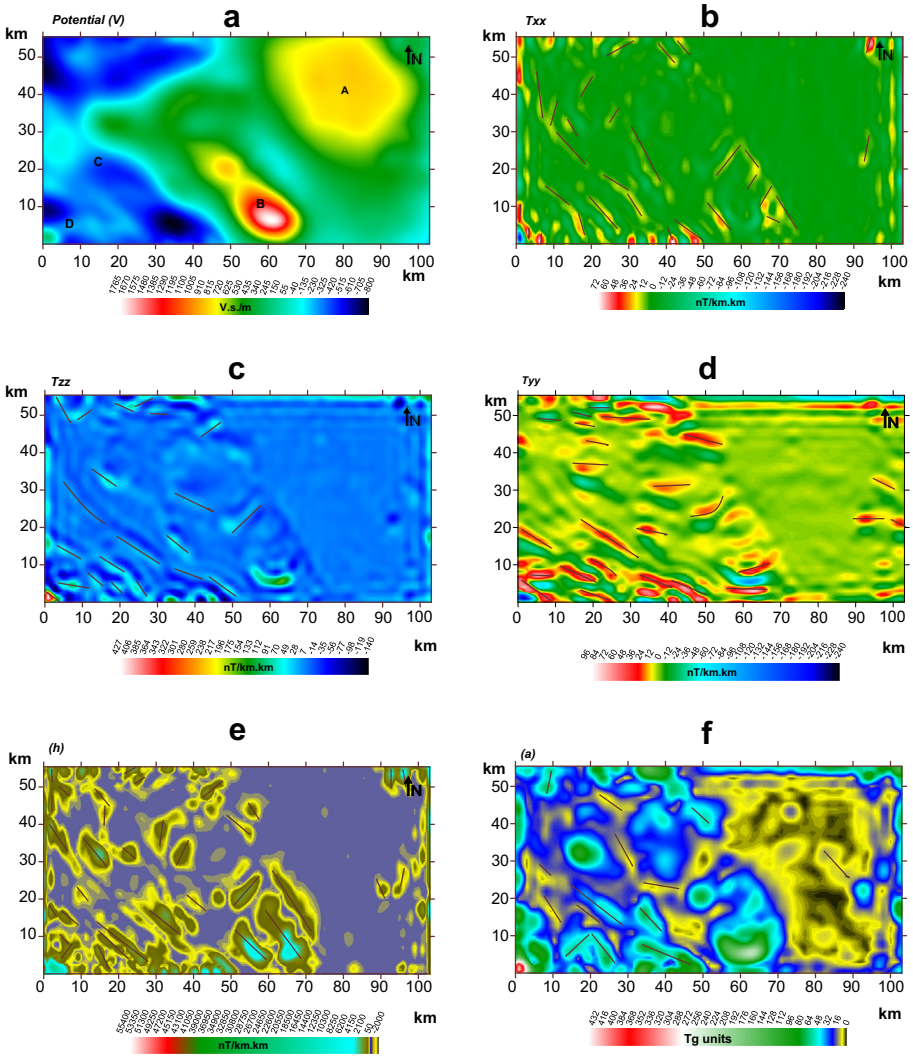

Fig. 5 Magnetic directional derivatives of Ar Rika area, Saudi Arabia. Regional linear/curvilinear features are posted on the maps.

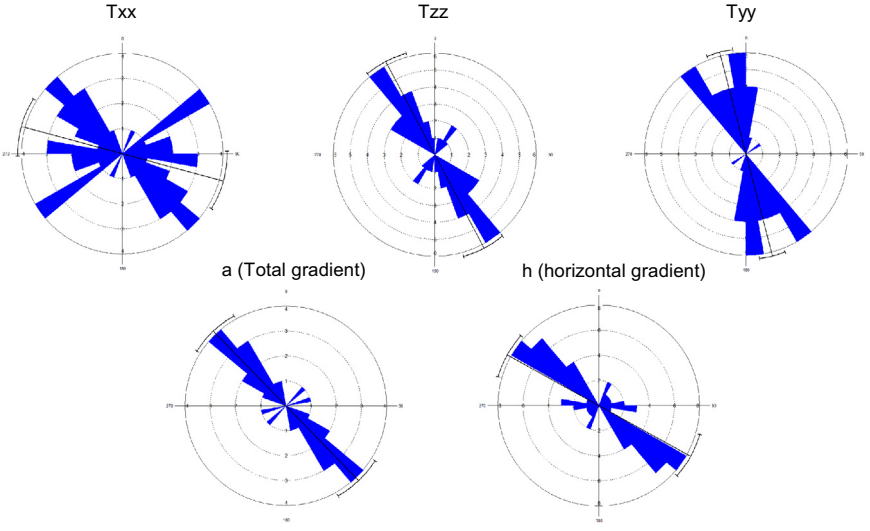

Fig. 6 Analysis of linear features and faults in the gradient maps.

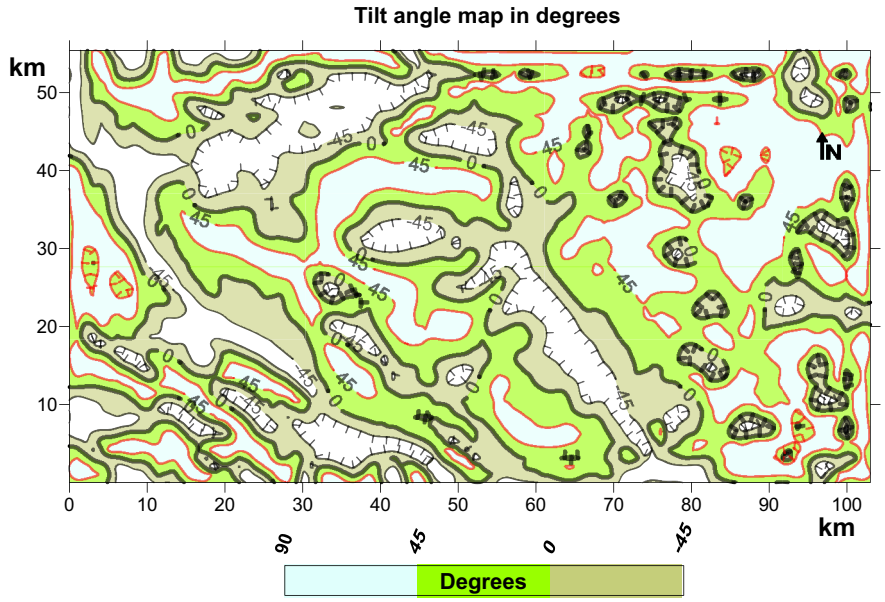

Fig. 7 Tilt angle map, Ar Rika area, Saudi Arabia.

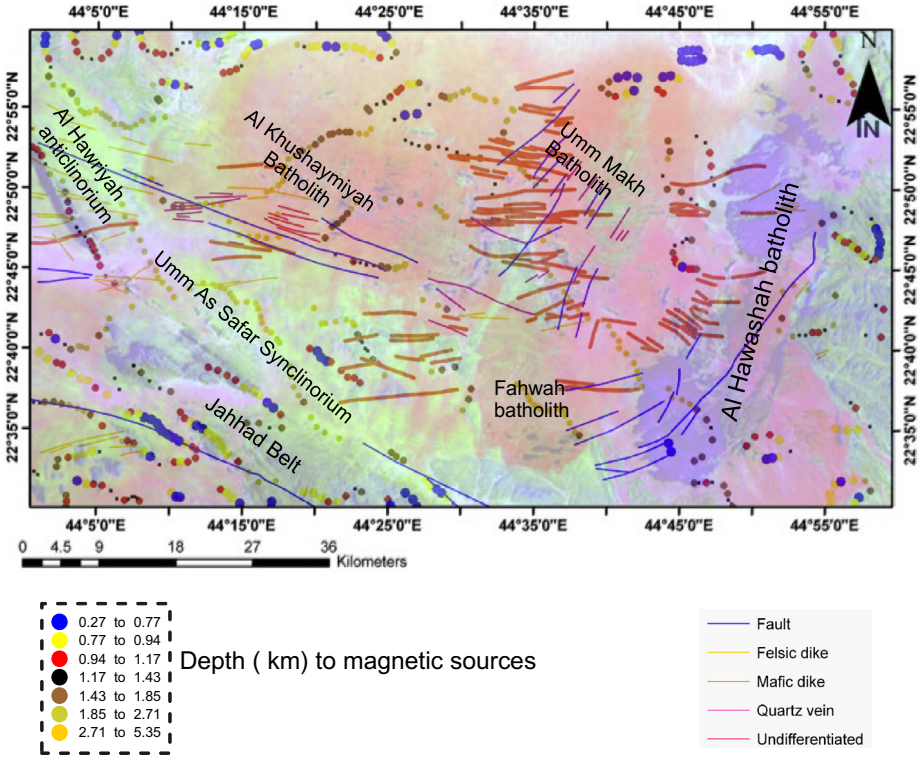

Fig. 8 Interpreted solution depths to source structures. Lineaments and surface faults interpreted from (PCA) image are posted, Ar Rika area, Saudi Arabia.

4. Depth estimation to causative sources

To estimate the depths of the magnetic source bodies in the study area assuming a vertical-contact model, we use the Tilt angle approach proposed by Salem and Williams (2007). The magnetic tilt angle is a normalized derivative based on the ratio of the vertical and horizontal derivatives of the RTP field and provides an intuitive means of understanding the variation in depth of the magnetic source (Salem et al., 2008). The method assumes that the source structures have vertical contacts, there is no remnant magnetization, and that the magnetization is vertical.

Following Nabighian (1972) and Salem and Williams (2007), the general expression for the vertical and horizontal

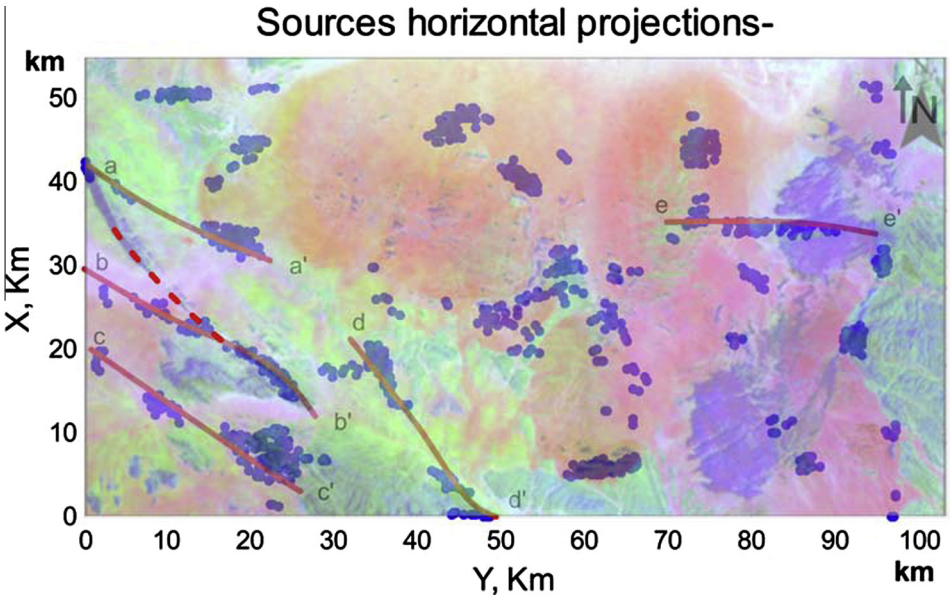

Fig. 9 Solutions of deconvolution algorithm for Ar Rika area, Saudi Arabia for $\tau = 0.05$.

derivatives of the magnetic field (M) over contacts located at a horizontal location of ($h = 0$) and a depth of z_0 is:

$$\frac{\partial M}{\partial h} = 2KFc \sin d \frac{z_c \cos(2I - d - 90) + h \sin(2I - d - 90)}{h^2 + z_c^2}, \quad (1)$$

$$\frac{\partial M}{\partial z} = 2KFc \sin d \frac{h \cos(2I - d - 90) + z_c \sin(2I - d - 90)}{h^2 + z_c^2}, \quad (2)$$

where, K is the susceptibility contrast at the contact, $\boldsymbol{F}$ the magnitude of the magnetic field, $c = 1 - \cos^2 I \sin^2 A$, A the angle between the positive h-axis and magnetic north, i the ambient field inclination, $\tan I = \tan i / \cos A$, d the dip (measured from the positive h-axis), and all trigonometric quantities are in degrees. When the contact in vertical (also the case for a vertical fault), the above equations are reduced to:

$$\frac{\partial M}{\partial h} = 2KFc \sin d \frac{z_c}{h^2 + z_c^2} \quad (3)$$

$$\frac{\partial M}{\partial z} = 2KFc \sin d \frac{h}{h^2 + z_c^2} \quad (4)$$

Combining the above two equations gives

$$\theta = \tan^{-1} \left[\frac{h}{z_c} \right] \quad (5)$$

Physically, the value for the tilt angle θ equals 0°, directly above the edges of the contact (fault) and equals 45° when $h = z_c$ and −45° when $h = -z_c$. Practically, the zero contour identifies the location of the edge or the contact and half of the physical distance between ±45° contour gives the depth to the source structure. The above technique is applied to

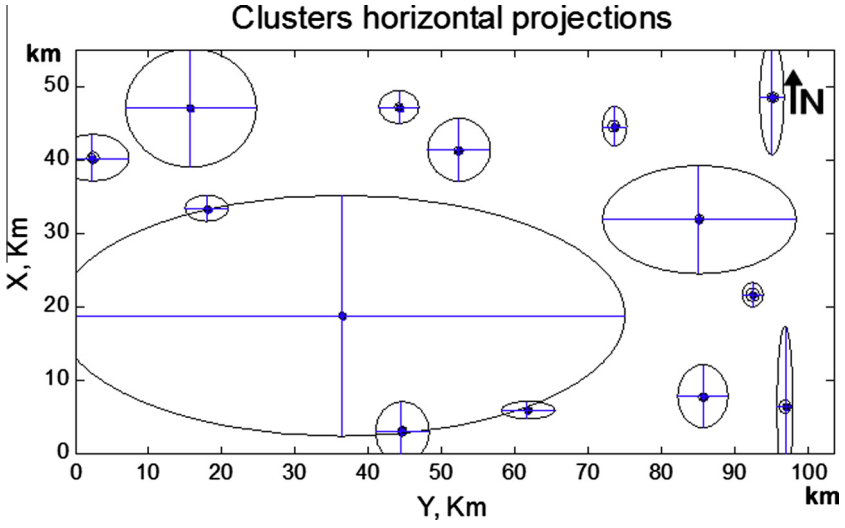

Fig. 10 Confidence intervals of horizontal position of centre of gravity of clusters with their depths for $\tau = 0.05$, $\rho_{mic} = 1$, $\rho_{mac.} = 1$, and $\rho_z = 0.5$.

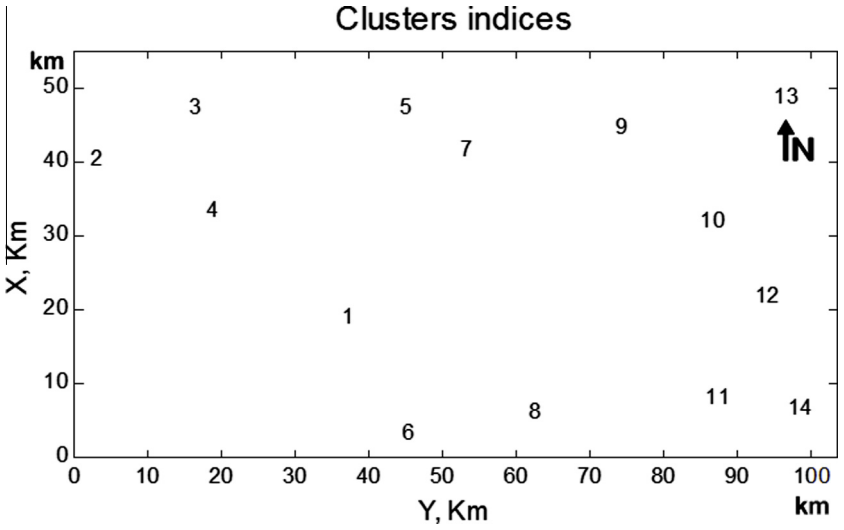

Fig. 11 Final clusters for Ar Rika area after the second clustering stage.

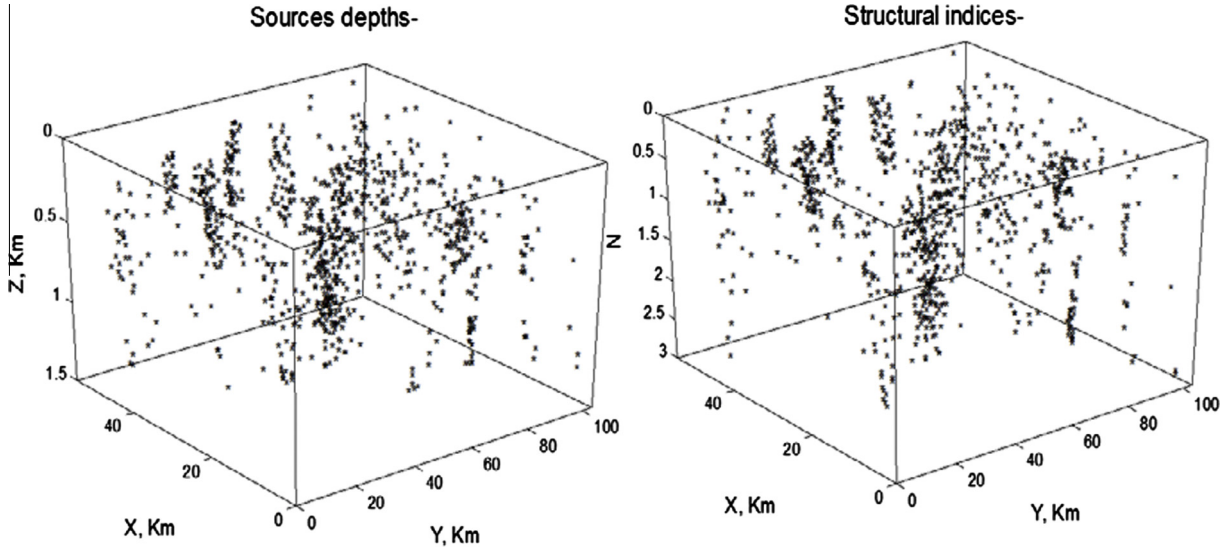

Fig. 12 Three-dimensional representation to the structural indices of the solutions and their corresponding depths, Ar Rika area, Saudi Arabia.

the RTP data from Ar Rika quadrangle. Fig. 7 shows the tilt angle map in degrees, the zero contour line identifies the location of possible vertical contacts or faults in the study area. Over shallow basement regions, the tilt angle map is characterized by high frequency magnetic anomalies and closely spaced contours. This is mainly concentrated at the south western corner (corresponds to anomalies C and D, shown in Fig. 5a). The north western boundary, and the central south of the region correspond to anomaly (B) shown in Fig. 5a. Tight physical distance between the $\pm 45°$ contours immediately indicate a shallow depth to basement/faults in this region typically less than 1.17 km. The depth to the Al Hawriyah anticlinorium is found to be 1.43 to 1.8 km, suggesting an intermediate depth to basements/or magnetic contacts. Minor deeper depths are distributed linearly and curvilinearly in this region. In contrast over the deep parts of the Wadi Ar Rika basin and Umm As Safar synclinorium, widely spaced contours are observed. Calculated depths in the Wadi range from 1.85 to 5.3 km. Fig. 8 shows the calculated depths to the possible sources in the study area. Lineaments and surface faults interpreted from Land sat (PCA) image are posted. All the above depths are from the survey level. The mean terrane clearance of the survey (150 m) should be taken into consideration for further detailed analysis using the mentioned depths.

5. Structural indices estimation using 3D Euler deconvolution

Euler deconvolution of magnetic anomalies is based on solving Euler's homogeneity equation of the form

$$(x - x_0)\frac{\partial F}{\partial x} + (y - y_0)\frac{\partial F}{\partial y} + (z - z_0)\frac{\partial F}{\partial z} = -NF \tag{6}$$

Table 2 Statistical analysis of clusters (first stage).

Cluster index	NumPoi	Xave	Xcon	Yave	Ycon	Zave	Zcon	Nave	Ncon
1.00	399	18.84	16.47	36.27	38.74	0.44	0.55	0.86	1.29
2.00	10	40.43	3.24	2.35	4.94	1.01	0.51	1.66	1.66
3.00	57	47.23	8.00	15.63	8.96	0.45	0.49	0.68	0.945
4.00	74	33.46	1.74	17.92	3.01	0.26	0.28	0.41	0.46
5.00	51	47.28	2.29	44.18	2.71	0.31	0.35	0.46	0.61
6.00	26	3.07	4.14	44.58	3.75	0.62	0.69	0.89	1.16
7.00	49	41.44	4.31	52.24	4.29	0.35	0.35	0.40	0.515
8.00	49	5.97	1.16	61.71	3.74	0.32	0.23	0.34	0.471
9.00	58	44.659	2.76	73.50	1.69	1.00	0.59	2.0	1.33
10.00	66	32.028	7.37	85.02	13.25	0.65	0.56	1.25	1.32
11.00	24	7.803	4.29	85.66	3.46	0.56	0.57	1.02	1.29
12.00	44	21.68	1.64	92.40	1.34	0.98	0.79	1.95	1.868
13.00	16	48.67	7.77	95.08	1.68	0.76	0.81	1.49	2.06
14.00	9	6.46	11.05	96.82	1.08	0.92	0.83	1.92	2.42

NumPoi: Number of points.
Xave: Average x value (km).
Xcon: Confidence interval for variable X (km).
Yave: Average Y value (km).
Ycon: Confidence interval for variable Y (km).
Zave: Average z value (km).
Zcon: Confidence interval for variable Z (km).
Nave: Average estimated structural indices for each cluster **SI**.
Ncon: Confidence interval for estimated structural indices N.

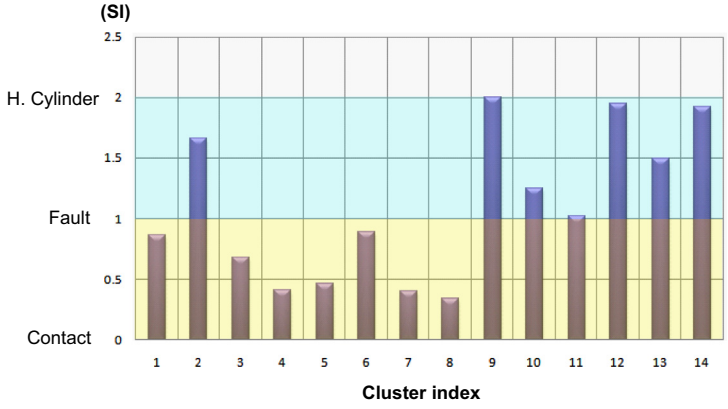

Fig. 13 Histogram of the **SI** calculated for the Ar Rika area.

where the homogenous function F is the observed field at location (x,y,z), caused by the anomalous source at location (x_0,y_0,z_0), and N, denoted as the structural index (**SI**), is a measure of the rate of change of the field with the distance (Reid, 1995; Reid et al., 1990; Thompson, 1982; FitzGerald et al., 2004). Selection of the correct (**SI**) is essential for the successful application of the method (Reid, 1995). In conventional Euler's technique, this is either based on experience, by trial and error, or using the index that produces the best clustering of solutions (Reid et al., 1990; Keating and Pilkington, 2002). This limitation constitutes the main subjective parameter when using Euler's equation. Other limitations come from ignoring the presence of a background field that influences the calculations. Several versions of the second limitation were presented by different authors (Hood, 1965; Ruddock et al., 1966; Thompson, 1982; Barbosa et al., 1999; Hsu, 2002). Modern approaches for solving such limitations are the linearization of the background field using Taylor series approximation in a moving window (Stavrev, 1997; Gerovska and Bravo, 2003). The subjectivity of the **SI** is solved by Gerovska and Bravo (2003) using unprescribed **SI** for a linear background in each moving window. The technique is fully automatic in estimating **SI** with a two stage clustering technique to achieve better imaging of the depths and horizontal locations of the causative sources. We apply the latter technique on RTP data of Ar Rika magnetic anomalies considering window of (6×16) grid points, for grid spacing in both directions of 1.04 km. The previously calculated partial derivatives of the field have been used. The necessary arguments and parameters for carrying out the deconvolution are, the acceptance criterion threshold value is chosen to be $\tau = 0.05$; $\rho_{mic} = 1$ (fraction of grid spacing parameter); $\rho_{mac.} = 1$ (used in the cluster fusion after mul-

tiplication by the maximum horizontal radius of confidence of all the clusters); and $\rho_z = 0.5$ (scaling factor). After the first and second cluster stages are applied, Fig. 9 is obtained.

The magnetic sources are located along five axes, (a–a′) has an orientation N68°W. The axis (b–b′) is N68°W, and it is probably split into a second segment (N 58°W) overlying the Al Hawriyah anticlinorium. The axis (c–c′) trends N59° W and form with the axis (b–b′) the lower and upper boundaries of the main Ar Rika shear Fault zone. The axis (d–d′) has an orientation of N40°W. Finally, the axis (e–e′) is trending nearly EW (N88°W). Several patches of shallow extrusive magnetic sources are distributed over the area and can be seen from the compact clustering of the solutions. Fig. 10 is the confidence interval of horizontal position of the center of gravity of clusters with their depths. Fig. 11 summarizes the final clusters for the Ar Rika region after the second clustering stage.

Generally, 14 clusters can be identified; each of them represents a set or groups of well clustered solutions. The automatically determined structural indices with their depths corresponding to the final clusters in Figs. 9 and 10 are shown in Fig. 12. The diagram to the left is the 3D distribution of calculated depths to each cluster solution. We display the source depths up to 1 km (shallow sources). The right diagram represents the 3D distribution of the automatically determined **SI** for these clusters. Table 2 summarizes the numerical solutions of Euler deconvolution. The estimated depth (z_{avr}) shows that most of the causative sources to the magnetic anomalies in the study area are shallow in nature. Maximum estimated depth is one km corresponding to cluster number 9 (Umm Makh batholiths), which at the same time has the maximum structural index (2.0) suggesting a plutonic extended magnetized source approximating a horizontal cylinder. All **SI**'s less than one according to FitzGerald et al. (2004) represent Faults and/or contact models (Table 2, Fig. 13), this is true for clusters (1, 3, 4, 6) that relate directly to the main trend of the Ar Rika fault zone. Whereas clusters 2, 9, 10, 11, 12, 13, and 14 represent massive magnetized sources having depth ranges from 650 m to 1 km. Particularly, cluster number 8 (depth 320 m, **SI** = 0.34) that corresponds to anomaly B (Fig. 4) represents a fault like structure.

6. Conclusions

Precambrian tectonic activity in the Wadi Ar Rika area that ended with epeirogenic movements is responsible for the very long fracture seams of the Najd fault system. These activities are reflected on the measured aeromagnetic field. The integrated analysis of the magnetic gradient tensor elements $\boldsymbol{T}_{xx}$, $\boldsymbol{T}_{yy}$, $\boldsymbol{T}_{zz}$, the horizontal gradient $\boldsymbol{h}$ and the total gradient $\boldsymbol{a}$, reveal a system of subsurface and surface lineaments and faults trending mainly NW-SE. Most of these linear features are shallow. Tilt angle method outlines the subsurface boundaries in the study area and estimates the depth of these boundaries. It ranges from 0.27 km to about 5 km. 3D Euler deconvolution is utilized to automatically estimate the source body shapes. Most of the estimated sources are linear/curvilinear. Few other extrusive sources are estimated to be clustered at different locations in the study area. Maximum depth calculated for these linear structures using the 3D Euler equation is about 1 km.

References

Abdelsalam, M.G., Stern, R.J., 1996. Sutures and shear zones in the Arabian–Nubian shield. J. Afr. Earth Sci. 23, 289–310.

Barbosa, V.C., Silva, J.B.C., Medeiros, W.E., 1999. Stability analysis and improvement of structural index estimation in Euler deconvolution. Geophysics 64 (1), 48–60.

Cole, J.C., Hedge, C.E., 1986. Geochronologic investigation of Late Proterozoic rocks in the northeastern Shield of Saudi Arabia. Deputy Ministry for Mineral Resources, Technical Record USGS-TR-05-5, Scale 1:1,000,000, 42p.

Delfour, J., 1980. Explanatory notes to the geologic map of the Wadi Ar Rika quadrangle, sheet 22G, Kingdom of Saudi Arabia. Ministry of Petroleum and Mineral Resources.

FitzGerald, D., Reid, A., Mc Inerney, P., 2004. New discrimination techniques for Euler deconvolution. Comput. Geosci. 30, 461–469.

Gerovska, D., Bravo, M.J.A., 2003. Automatic interpretation of magnetic data based on Euler deconvolution with unprescribed structural index. Comput. Geosci. 29, 949–960.

Hood, P.J., 1965. Gradient measurements in aeromagnetic surveying. Geophysics 30 (5), 891–902.

Hsu, S.K., 2002. Imaging magnetic sources using Euler's equation. Geophys. Prospect. 50 (1), 15–25.

Johnson, P.R., 1996. Geochronologic and Isotopic Data for Rocks in the East-Central Part of the Arabian Shield Stratigraphic and Tectonic Implications Ministry of Petroleum and Mineral Resources. Directorate General of Mineral Resources, Jeddah, Saudi Arabia.

Johnson, P.R., Woldehaimanot, B., 2003. Development of the Arabian–Nubian shield: perspectives on accretion and deformation in the East African Orogen and the assembly of Gondwana. In: Yoshida, M., Windley, B.F., Dasgupta, S. (Eds.), Proterozoic East Gondwana: Supercontinent Assembly and Breakup. Geological Society, London, Special Publication, pp. 289-325.

Kanaan, F.M., 1979. The Geology, petrology, and geochemistry of the granitic rocks of Jabal Al Hawshah and vicinity, Jabal Al Hawshah Quadrangle, Kingdom of Saudi Arabia. Saudi Arabian Directorate General of Mineral Resources Bulletin No. 23, 114pp, 152 ills., 18 tables, 1 pI.

Keating, P., Pilkington, M., 2002. A comparison of some interpretation techniques for magnetic data. In: SEG Int'l Exposition and 72nd Annual Meeting, Salt Lake City, Utah, October 6–11, 2002.

Mogren, S., Al Amri, A.M., Al-Damegh, K., Fairhead, D., Jassim, S., Algamdi, A., 2008. Subsurface geometry of Ar Rika and Ruwah faults from gravity and magnetic surveys. Arab. J. Geosci. 1, 33–47.

Moore, J.M., Allen, P., Wells, M.K., Howland, A.F., 1979. Tectonics of the Najd transcurrent fault system, Saudi Arabia. J. Geol. Soc. Lond. 136, 441–454.

Nabighian, M.N., 1972. The analytic signal of two-dimensional magnetic bodies with polygonal cross-section; its properties and use for automated anomaly interpretation. Geophysics 37, 507–517.

Nehlig, P., Genna, A., Asirfane, F., 2002. A review of the Pan-African evolution of the Arabian Shield. GeoArabia 7, 103–124.

Phillips, J.D., Hansen, R.O., Blakely, R.J., 2007. The use of curvature in potential-field interpretation. Explor. Geophys. 38, 111–119.

Reid, A.B., Allsop, J.M., Granser, H., Millett, A.J., Somerton, I.W., 1990. Magnetic interpretation in three dimensions using Euler deconvolution. Geophysics 55 (1), 80–91.

Reid, A.B., 1995. Euler deconvolution: past, present and future—a review. In: 65th Ann. Internat. Mtg. Soc. Expl. Geophys., Expanded Abstracts, pp. 272–273.

Richards, J.A., Jia, X., 1999. Remote Sensing Digital Image Analysis – An Introduction, third ed. Springer-Verlag, Berlin, p. 363.

Ruddock, K.A., Slack, H.A.B, Breiner, S., 1966. Method for determining depth and falloff rate of subterranean magnetic disturbances utilizing a plurality of magnetometers. US Patent 3,263,161.

Salem, A., Williams, S., Fairhead, D., Smith, R., Ravat, D., 2008. Interpretation of magnetic data using Tilt-Angle derivatives. Geophysics 73 (1), P.L1–P.L10.

Salem, A., Williams, S., 2007. Tilt-depth method: a simple depth estimation method using first-order magnetic derivatives. Lead. Edge, 1502–1505.

Stern, R.J., 1985. The Najd Fault System, Saudi Arabia and Egypt—a late Precambrian rift-related transform system. Tectonics 4, 497–511.

Stavrev, P.Y., 1997. Euler deconvolution using differential similarity transformations of gravity or magnetic anomalies. Geophys. Prospect. 45 (2), 207–246.

Thompson, D.T., 1982. EULDPH: a new technique for making computer-assisted depth estimates from magnetic data. Geophysics 47 (1), 31–37.